Ag–Ag2S Hybrid Nanoprisms: Structural versus Plasmonic Evolution

Shahjamali, Mohammad M.; Zhou, Yong; Zaraee, Negin; Xue, Can; Wu, Jinsong; Large, Nicolas; McGuirk, C. Michael; Boey, Freddy; Dravid, Vinayak; Cui, Zhifeng; Schatz, George C.; Mirkin, Chad A.

2016

Shahjamali, M. M., Zhou, Y., Zaraee, N., Xue, C., Wu, J., Large, N., et al. (2016). Ag–Ag2S Hybrid Nanoprisms: Structural versus Plasmonic Evolution. ACS Nano, 10(5), 5362-5373.

https://hdl.handle.net/10356/84975

https://doi.org/10.1021/acsnano.6b01532

Ag-Ag_2S Hybrid Nanoprisms: Structural *vs.* Plasmonic Evolution

Mohammad M. Shahjamali,[†,‡,⊥,¶] *Yong Zhou,*[†,∥,¶] *Negin Zaraee,*[†,⊥] *Can Xue,*[‡] *Jinsong Wu,*[§] *Nicolas Large,*[†] *C. Michael McGuirk,*[†] *Freddy Boey,*[‡] *Vinayak Dravid,*[§] *Zhifeng Cui,*[∥] *George C. Schatz,*[†,*] *Chad A. Mirkin*[†,§,*]

[†] Department of Chemistry and International Institute for Nanotechnology, Northwestern University, 2145 Sheridan Road, Evanston, IL 60208, USA

[‡] School of Materials Science and Engineering, Nanyang Technological University, 50 Nanyang Avenue, Singapore 639798, Singapore

[⊥] Harvard John A. Paulson School of Engineering and Applied Sciences, Harvard University, Cambridge, Massachusetts 02138, United States

[§] Department of Materials Science and Engineering and NUANCE Center, Northwestern University, Evanston, Illinois 60208, United States

[∥] Department of Physics, Anhui Normal University, Wuhu, Anhui 241000, China

KEYWORDS: sulfidation, anisotropic reaction, metal-semiconductor, hybrid nanoplate, discrete dipole approximation (DDA), anisotropic core-shell nanoparticles

*To whom correspondence should be addressed. E-mail: chadnano@northwestern.edu and g-schatz@northwestern.edu. ¶These authors contributed equally.

ABSTRACT

Recently Ag-Ag_2S hybrid nanostructures have attracted a great deal of attention due to their enhanced chemical and thermal stability, in addition to their morphology- and composition-dependent tunable local surface plasmon resonances. Although Ag-Ag_2S nanostructures can be synthesized *via* sulfidation of as-prepared anisotropic Ag nanoparticles, this process is poorly understood, often leading to materials with anomalous compositions, sizes, and shapes, and consequently, optical properties. In this work we use theory and experiment to investigate the structural and plasmonic evolution of Ag-Ag_2S nanoprisms during the sulfidation of Ag precursors. The previously observed red-shifted extinction of the Ag-Ag_2S hybrid nanoprism as sulfidation occurs contradicts theoretical predictions, indicating that the reaction does not just occur at the prism tips as previously speculated.

Our experiments show that sulfidation can induce either blue- or red-shifts in the extinction of the dipole plasmon mode, depending on reaction conditions. By elucidating the correlation with the final structure and morphology of the synthesized Ag-Ag_2S nanoprisms, we find that, depending on the reaction conditions, sulfidation occurs on the prism tips and/or the (111) surfaces, leading to a core(Ag)-anisotropic shell(Ag_2S) prism nanostructure. Additionally, we demonstrate that the direction of the shift in the dipole plasmon is a function of the relative amounts of Ag_2S at the prism tips and Ag_2S shell thickness around the prism.

Binary nanoparticle structures of well-defined shape, size and composition have attracted significant attention due to synergistic properties that arise from the interactions between the individual components.[1-6] Promising examples of such nanostructures include metal-semiconductor hybrid nanocrystals, in which metallic and semiconductor components are coupled synthetically to produce physical properties that transcend those associated with structures comprised of their individual components.[7-16] In particular, these hybrid nanostructures allow for the coupling of quantum confinement effects for excitons in the semiconducting portion[17] and shape-dependent localized plasmon excitation in the metallic portion,[18] which leads to the optimization of plasmon enhanced emission or absorption for applications in electronic and solar devices,[19,20] as well as in photocatalysis.[21]

Over the past decade, considerable progress has been made in the synthesis of noble metal-semiconductor heterodimer nanostructures, including Au-CdSe,[7,15,22] Ag-ZnO,[23] Pt-CdS,[24,25] Au-Ag_2S,[26] Ag-Cu_2O[27] and Ag-Ag_2S.[1-3] Although the majority of such heterodimers are synthesized by growing a shell of the noble metal onto the semiconductor components, in the case of silver nanoparticles, it is possible to chemically convert portions of anisotropic silver nanostructures to the corresponding semiconductor material (Ag_2S, Ag_2Se, Ag_2Te),[28,29] thus allowing for the synthesis of hybrid structures beyond the conventional uniform core-shell motif. Of the known Ag-based hybrid nanostructures, Ag-Ag_2S is of particular interest due to the unique properties of Ag_2S.[28-31] Specifically, Ag_2S is a direct narrow-band-gap semiconductor (1 eV), and also an effective superionic conductor, in which Ag^+ has considerable mobility in a cationic vacancy-rich phase.[30,31] In addition, due to its high optical absorption coefficient, chemical stability and efficient photoluminescence, Ag_2S has been used in solar cells,[32,33] as well

as a photocatalyst,[34-36] biosensor,[3] antibacterial material,[2] photoconductor,[22] IR detector,[37] superionic conductor[38-40] and bioimaging agent.[41-43]

Because of the potential of these hybrid nanomaterials, recently, the synthesis and characterization of such systems has been extensively investigated.[3,44,45] Fang and coworkers studied the sulfidation of Ag nanocubes both experimentally and theoretically.[44] Importantly, they were able to elucidate a correlation between the structure and plasmonic properties of the nanocubes during the sulfidation reaction. Additionally, Zeng *et al.* demonstrated a new approach to the corner-site-selective sulfidation of Ag nanoprisms and nanocubes.[45] They showed that as the sulfidation process takes place: i) the triangular shape is essentially unchanged with the Ag-to-Ag_2S conversion starting nearly exclusively from the corners, and ii) the in-plane dipole plasmon peak red shifts continuously. The authors speculated that the red-shift was a result of the higher dielectric constant of Ag_2S, but no experimental evidence to support this claim was provided. Previous studies[46,47] showed that truncation of the triangular corner leads to blue-shifting of the in-plane dipole plasmon peak, which seemingly conflicts with the large red-shifting reported by Zeng *et al*.[45] One possible explanation for this contradiction is that the observed red-shifting is caused by the high-refractive-index Ag_2S at the prism tips (where $n + k\mathrm{i} \approx 3.1 + 0.8\mathrm{i}$), which overwhelms the expected blue-shifting from corner truncation. Another possibility is that the interface between the metal (Ag) and semiconductor (Ag_2S) in the nanoparticle may give rise to a new plasmonic state associated with additional carriers in the semiconductor that dominates the spectrum. Therefore, in order to explain these intriguing physical phenomena, we have sought to elucidate the chemical and physical contributions to the photophysical properties of Ag-Ag_2S hybrid nanoprisms.

By using multiple characterization techniques, in addition to theoretical calculations, we have studied the correlation between morphology, composition, and LSPR wavelength for the triangular Ag nanoprisms after various degrees of sulfidation. This study shows that in addition to sulfidation occurring at the prism tips, the reaction also proceeds on the triangular flat surfaces of the prisms, leading to a core-anisotropic shell Ag-Ag_2S nanoprism structure (*i.e.,* the Ag_2S thickness is different on different surfaces of the Ag core; as shown in Scheme 1D), in which the plasmon can be blue- or red-shifted depending on morphological changes that can be tailored by reaction conditions. This work provides a new fundamental understanding of the sulfidation of anisotropic Ag nanoprisms, and more generally suggests a reaction pathway for making anisotropic nanoscale systems that may have applications in such areas as electronics, solar energy conversion, and photocatalysis.

Results and discussion

For this study, triangular silver nanoprism precursors with tailorable LSPR wavelengths were prepared through a plasmon-mediated photochemical route.[48-51] Sulfidation of the Ag nanostructures was realized by reacting the Ag nanoprism precursors with aqueous sodium polysulfide (Na_2S_x), similar to the methodology outlined by Zeng *et al.*[45] Specifically, an aqueous solution of Na_2S_x was added in precise amounts to a dispersion of Ag nanoprisms. The sulfidation reaction was monitored by recording extinction spectra of the reaction solution, monitoring Na_2S_x concentration and reaction time.

Since the plasmonic spectral properties of metal nanocrystals are known to be affected by the nanocrystal size, shape, composition, and environment, the different spectra recorded during the sulfidation process provides important information pertaining to the morphological characteristics of the resulting particles. Namely, we have observed that in contrast with previous

studies,[45] by using different concentrations of Na_2S_x during the sulfidation of Ag nanoprisms, we can control spectral shifts of the dipolar LSPR band of the resulting Ag-Ag_2S hybrid nanoprisms. Based on the empirical data gathered, we have attributed the observed sulfidation products to three distinct chemical pathways involving low, intermediate, and high S_x^{2-} concentrations.

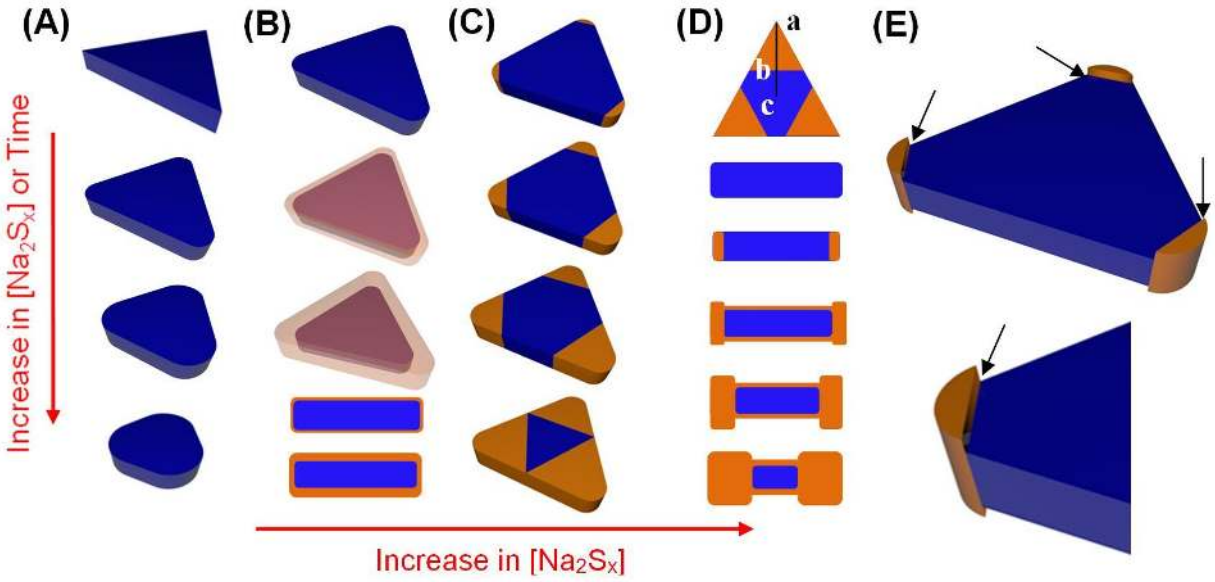

Scheme 1. (A-C) Proposed pathway of sulfidation processes as a function of Na_2S_x concentration: (A) $C < 30$ µM (B) 30 µM $< C <$ 100 µM (C) $C > 150$ µM. (D) Nanoprisms' side view used to illustrate the change in height of hybrid nanoprisms for panel C. The top scheme defines the sulfidized section (SS) parameter, which is a radial ratio of Ag_2S and Ag from the tip of nanoprism to its center (*ab/ac*). (E) Diffusion sites of S_x^{2-} in the $C > 150$ µM range at the interface of Ag and Ag_2S are illustrated by the black arrows.

I: Low S_x^{2-} Concentration

Surprisingly, we found that when the sulfidation was carried out with lower Na_2S_x concentrations (C <30 μM), the spectral evolution of the hybrid nanoprism behaves differently (blue-shifts) from when high concentrations of Na_2S_x (C >150 μM) are used (Figure 1A). At low concentrations, the LSPR band of the prism blue-shifts after addition of Na_2S_x, which is a behavior not observed in earlier work.[45] S_x^{2-} oxidizes the Ag nanoprisms, leading to rounding and truncation of the tips of each nanoprism (Figure 1C). The etching of the prism tips as opposed to the faces of the prism is due to the high stability of the (111) planes relative to atoms in the sharp tips and edges of the nanoprisms.

II: Intermediate S_x^{2-} Concentration

Extinction spectra and TEM images of the particles (Figure 1D and F) at intermediate concentrations (30 < *C* < 100 μM) similarly show that blue-shifts and nanoprism truncation still occurs, but not to the extent at which it occurs in the low concentration regime. Interestingly, after the reaction, the truncated nanoprisms have a greater tendency to aggregate and form stacks which is not typical for the Ag nanoprisms stabilized with BSPP and trisodium citrate as the capping agent.

The silver ions in solution, which are the product of silver nanoprisms being etched and truncated, will react with the sulfide ions in the intermediate concentration range (as the concentration of sulfur ions is higher than the low concentration case) and create sub-10 nm spherical Ag_2S nanoparticles (Figure 1F). We found that these sub-10 nm nanoparticles will not form in higher concentrations of sulfur. This is because in higher concentrations of sulfur the etching and truncation of nanoprisms will not be as intense as in low and intermediate

concentration regimes, and therefore, there is not enough silver ions in the solution to initiate formation of the sub-10 nm spherical Ag_2S nanoparticles.

III: High S_x^{2-} Concentration

At higher concentrations (C >150 μM) of Na_2S_x, the LSPR peak corresponding to the longest excitation wavelength (in-plane dipole mode according to previous works)[46,47] shows clear red-shifting. The experimental extinction spectra acquired for the sulfidation reaction at these concentrations show that the dipole resonance exhibits large red-shifts (~170 nm) and a rapid drop in extinction from 0.84 to 0.11 (Figure 2A,B). This spectral evolution occurred

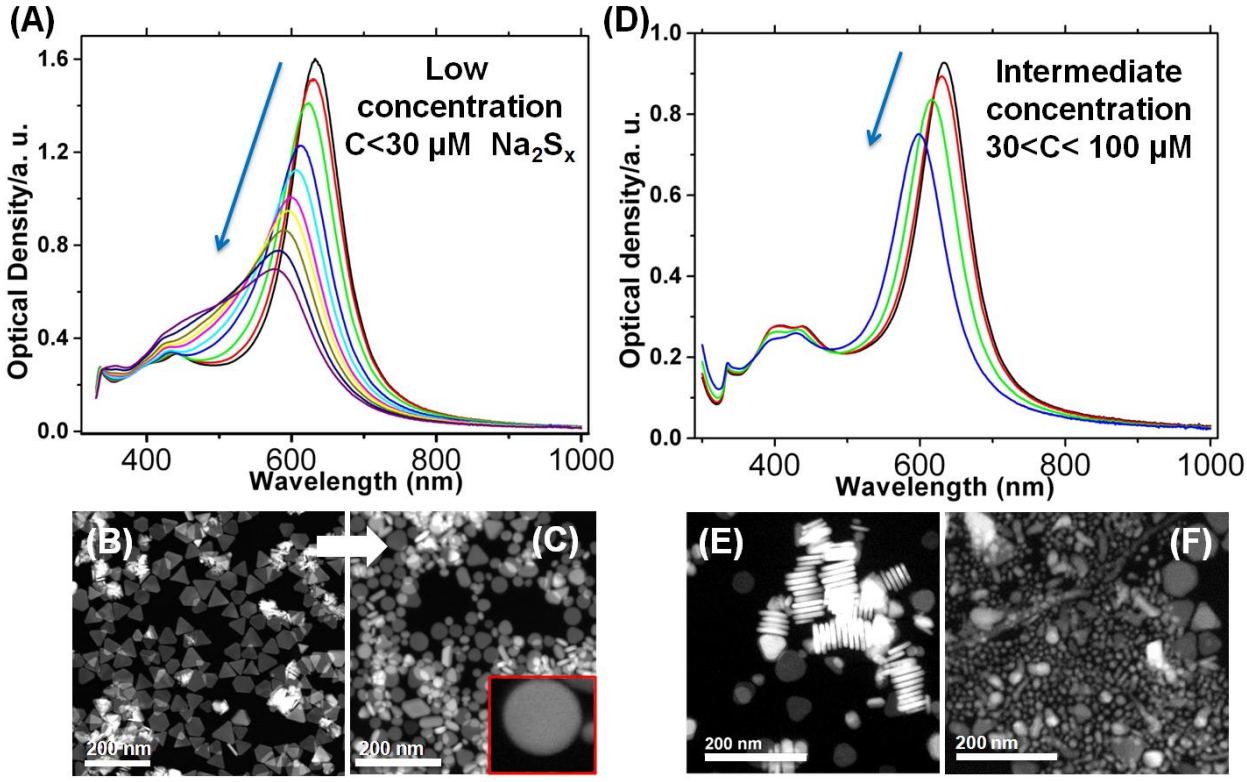

Figure 1. (A) Spectral changes over the course of sulfidation of the Ag nanoprisms at an overall Na_2S_x concentration below 30 μM (low concentration). Each spectrum is taken after addition of successive doses of Na_2S_x to reach a concentration of ~2 μM in the reaction vessel. STEM images of: (B) The initial triangular nanoprism, and (C) Nanodisc products obtained after the sulfidation reaction. The inset is a magnified circular nanodisc from the same batch of sample. (D) Extinction spectra at the intermediate concentration regime ($30 < C < 100$ μM). STEM images of: (E) Slow-dried nanoparticles without any modification show their high tendency to agglomerate in the form of stacks which is not common for silver nanoprisms stabilized with trisodium citrate and BSPP, and (F) Sub-10 nm spherical Ag_2S nanoparticles observed in the intermediate concentration range.

within 5 min of the reaction being started. After ~10 min, the reaction slows down, but still continues as indicated by changes in the absorption of the Ag-Ag_2S nanoprisms. After 18 h, the red-shifting peak of Ag-Ag_2S nanoprisms at ~820 nm, gradually disappears and the intensity plateaus, revealing the complete conversion of all metallic Ag to Ag_2S (Figure S1A). Sulfidation products collected at 0, 1, 2 and 5 min of the reaction were characterized by UV-Vis spectroscopy, scanning transmission electron microscopy (STEM), elemental mapping and X-ray photoelectron spectroscopy (XPS).

STEM images of particles show that the nanostructures remain triangular with smooth facets during the course of sulfidation in the high concentration range. A considerable amount of Ag in each nanostructure is converted into Ag_2S within the first 5 min of the reaction. In the STEM images (Figure 3A-C), the contrast observed between the tips and center of the nanoprism products suggests that Ag is converted to silver sulfide at the tips. With increasing reaction time, the sulfidized regions are enlarged and extended from the three tips toward the center of the nanoprism. To accurately quantify Ag_2S conversion, in addition to nanoprism dimensions we define another parameter, the sulfidized section (SS), which is a radial ratio of Ag_2S and Ag from the tip of nanoprism to its center (Scheme 1D). The *SS* value for three sulfidation stages of the experiments (1, 2 and 5 min) were measured and averaged, yielding SS = 17.9, 36.7, and 49.7%. These values were obtained by measuring at least 50 nanoprisms that were both triangular in shape and had a Ag-Ag_2S boundary parallel to the bases of the Ag nanoprism. Note that the hexagonal, disc-shape nanoparticles are not counted due to the complexity of the measurement and non-site-selective diffusion of S_x^{2-} in those morphologies.

Elemental mapping was then performed to reveal the composition changes during sulfidation (Figure 3D-F). Sulfur is clearly detected at the three tips of the nanoprism,

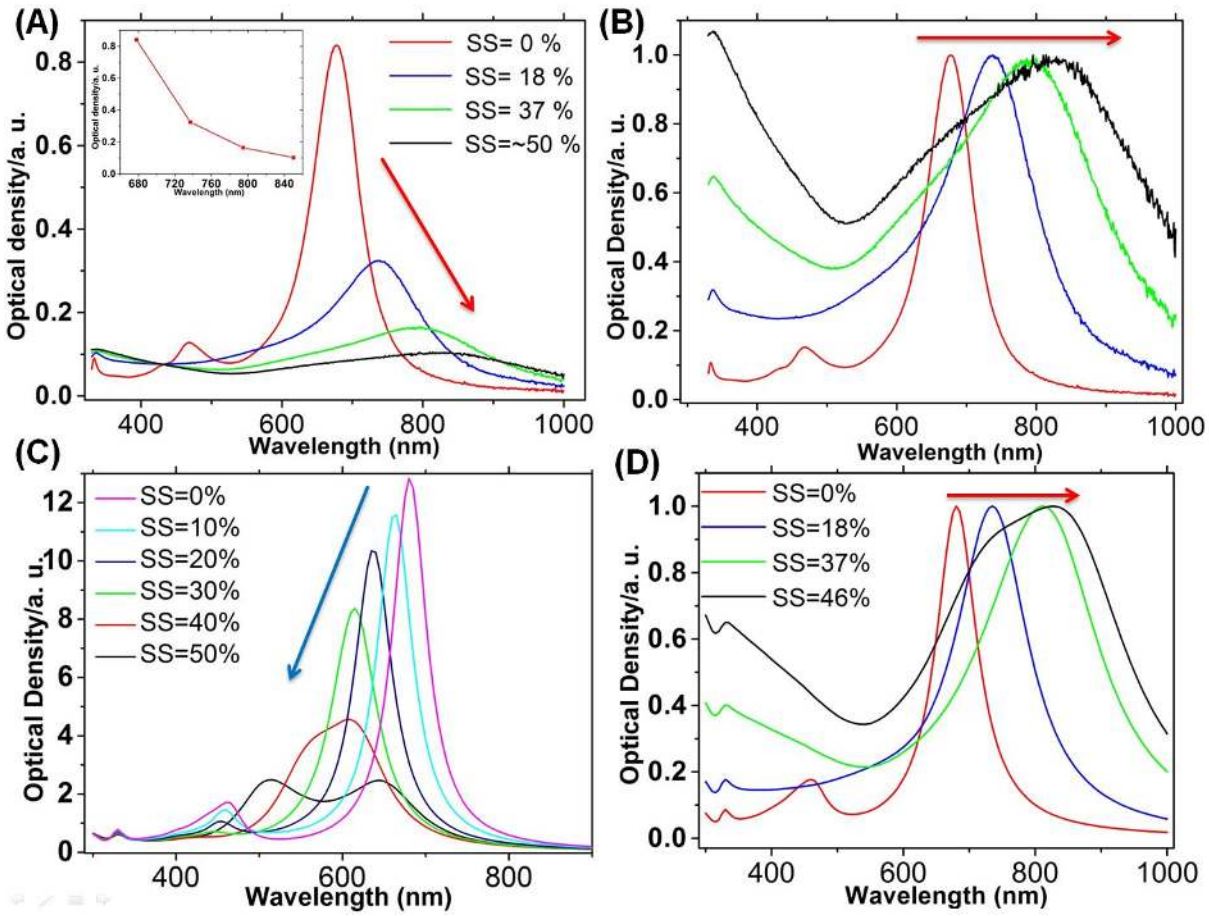

Figure 2. (A-B) Experimental and (C-D) calculated extinction spectra over the course of Ag nanoprism sulfidation at a S_x^{2-} concentration greater than 150 μM. The arrows show the direction of spectra shifting. (A) Representative extinction spectra of the reaction mixture recorded at 0, 1, 2 and 5 min. To reveal more clearly the spectral changes during the sulfidation process, the peak positions *vs.* intensity is plotted in the inset. (B) Normalized spectra of panel A. (C) Calculated extinction spectra over the course of sulfidation (with increasing the *SS* value) for the *tip-converted model* shows a blue-shift trend, which is the opposite trend in comparison to the experimental data mentioned in panel A and B above. (D) Calculated extinction spectra over the course of sulfidation of the Ag nanoprism considering the *core-anisotropic shell model*. This shows the dipole LSPR for each stage of sulfidation at 680, 734, 801 and 827 nm for Ag_2S shell thicknesses of 0, 0.6, 1.35 and 1.55 nm, respectively.

confirming again that sulfidation is initiated at the highly reactive tips of the Ag nanoprisms. The tips and vertices of the nanoprisms are obvious locations for initiation of sulfidation. In general at the sharp vertices, the Ag atoms have a smaller coordination number, and are less capped by stabilizing molecules, which makes them more prone to reaction with halides, oxygen, and sulfur containing species in solution.

Note that the molar volume of Ag_2S is 69.9% higher than Ag (34.3 cm^3/mol *versus 10.3* cm^3/mol), which makes the Ag_2S tip volume on average 69.9% larger in volume than the original Ag portion of each nanoprism after the reaction. For small nanoprisms (~50 nm) expansion of the Ag_2S tips is not observable under TEM (Figure 3A, M), consistent with a previous report,[45] which might be due to the instability of silver chalcogenides under the electron beam.[52] However, when we characterized the nanoprisms with AFM, both small (<100 nm) and large nanoparticles (~200 nm) showed a larger height profile at the tips indicating the Ag_2S phase expansion (Figure 3G-L).

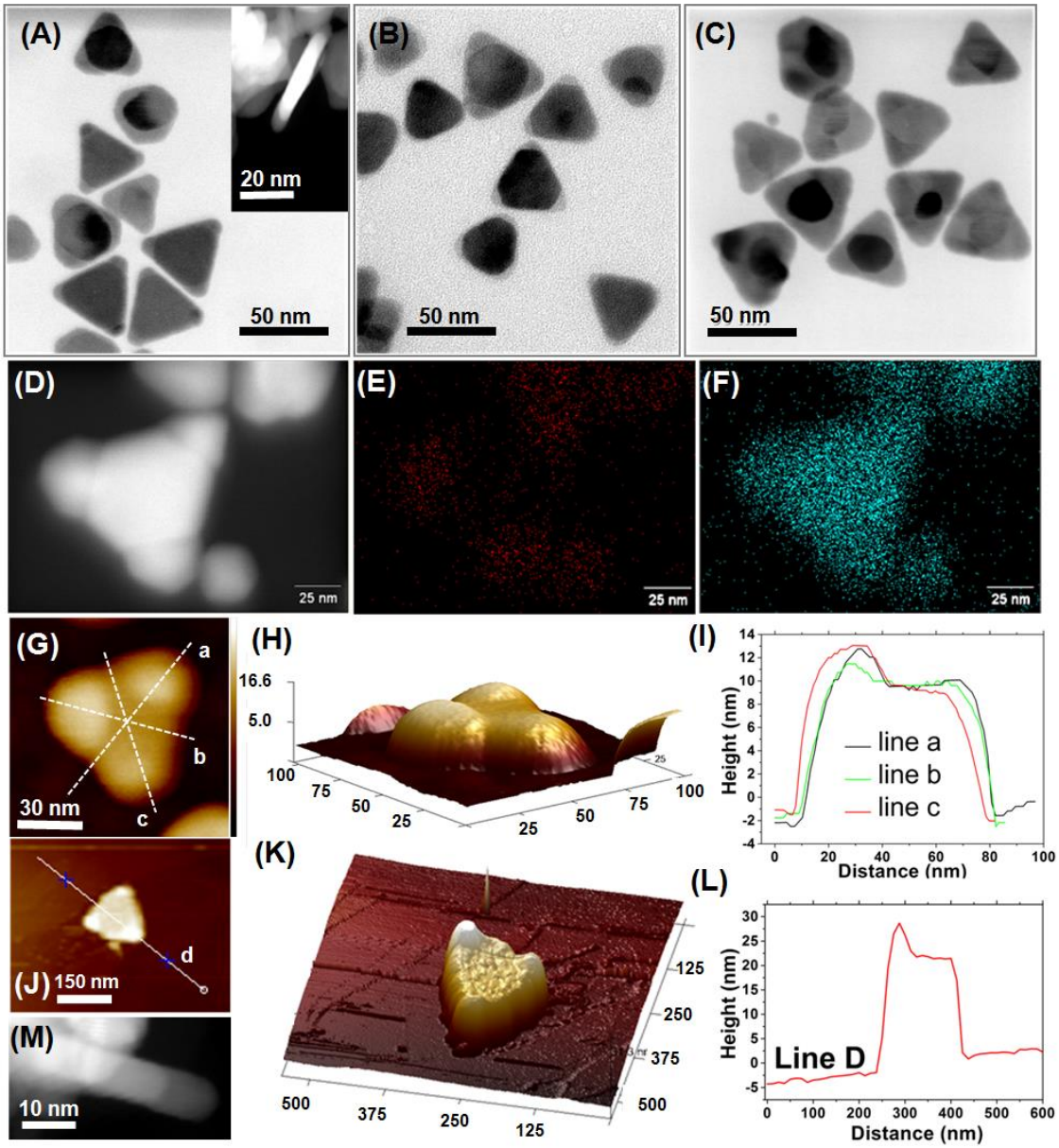

Figure 3. (A-C) TEM images of the Ag-Ag_2S hybrid nanoprisms obtained after the sulfidation reaction has progressed for: (A) 1, (B) 2 and (C) 5 min. The scale bar for panel A, B and C is 50 nm as illustrated in panel C. The dark region in the center corresponds to Ag, while the gray regions at the tips correspond to Ag_2S. The inset in panel A is a side view of an Ag-Ag_2S nanoprism. (D-F) Elemental maps (Red = S, blue = Ag) recorded on a single Ag-Ag_2S nanoprism. (G-I) AFM image, 3D model and height profile of a ~50 nm Ag-Ag_2S nanoprism show the increase in height on the tips of the nanoparticle. (J-L) AFM image, 3D model and height profile of an Ag-Ag_2S hybrid nanostructure with ~200 nm edge-length shows 10 nm height differences between the Ag and Ag_2S components. (M) STEM images of the side view of the Ag-Ag_2S hybrid nanoprism do not reveal any height difference between the Ag and Ag_2S parts for the small size (<100 nm) nanoprisms.

Computational Modeling of Sulfidation and Oxidative Etching

To clarify the role played by sulfidation of the Ag tips in the LSPR shifting, Discrete Dipole Approximation (DDA) simulations were performed for the Ag-Ag_2S nanoprisms using dimensions similar to those measured for these particles.

We first calculated the extinction spectrum of bare Ag nanoprisms, based on experimentally determined size parameters (Figure S1) similar to our previous studies.[46] The average edge-length (*L*) of the fully formed triangular Ag nanoprisms was 51±10 nm, the average prism thickness (*H*) was 7±1 nm and the corner of the triangle was found to be rounded with a radius (*R*) of 6±0.5 nm (Figure S1D), as determined by TEM. Within the range of wavelengths considered here, three LSPR peaks can be observed, which can be assigned (starting at the longest wavelength) to the in-plane dipole mode, the in-plane quadrupole mode and the out-of-plane quadrupole mode according to previous studies.[46,47,53-57] The calculated spectrum of pure nanoprisms (Figure S1C) is in good agreement with the experimental UV-Vis spectrum (Figure S1B), which confirms the accuracy of the measured dimensional parameters.

The SS value increases during the sulfidation process both by increasing Na_2S_x concentration or reaction time. The radius (*R*) for tip rounding is fixed at its initial value (*i.e.,* that of the bare Ag nanoprism) in all simulations due to its minor change after sulfidation (in the high concentration regime) and also its minor influence on the LSPR wavelength once the tips are sulfidized.

In the next step the effect of changing the *L, H* and *SS* parameters is theoretically studied, as these parameters respectively represent three different possible morphology pathways: i) edge conversion, ii) top and bottom facet conversion and iii) tip conversion of Ag nanoprisms into Ag_2S (Figure 4A- C respectively). As a computational control, the same structural changes were

considered for a pure silver nanoprism by substitution of the Ag_2S component with vacuum (Figure S2).

The growth of Ag_2S at the tips observed in the experiment was imitated by increasing the SS value defined above. As illustrated in Figure S2C, truncation of the prism tips for a bare silver prism blue-shifts the dipole LSPR peak. The experimentally observed growth of Ag_2S at the tips was then modeled by replacing the tips with Ag_2S rather than vacuum and with increasing the *SS* value. The spectral evolution is illustrated in Figure 2C and 4C with different *SS*. In spite of the larger index of the Ag_2S, this does not change the blue-shifting trend mentioned above. Thus, the experimentally observed red-shifting generated during the sulfidation process should not be attributed to sulfidation itself, and, therefore, suggests that some unknown or omitted morphological change in the Ag nanoprism is responsible for the observed red-shifting.

To explore the origin of the red-shifting, we studied the influence of reducing the edge length (L) and thickness (H) of the Ag component (due to Ag_2S conversion), both of which may occur during the sulfidation process. It was found computationally that conversion of either the edges or the top and bottom facets of the Ag component can lead to red-shifting (Figure 4A- B). Note that the morphological change in Figure 4A is not synthetically feasible due to the anisotropic nature of the silver nanoprism, but top and bottom facet and tip conversion (Figure 4B-C, respectively) are probable, and have been observed in our experiments.

Interestingly, our calculations suggest that the shift of the dipolar LSPR is more sensitive to absolute changes in prism thickness rather than the edge length. For instance, as shown in Figure 4B, in order to achieve a red-shift of 150 nm, an approximately 25 nm (or 50%) Ag_2S conversion in edge length of the Ag component is needed. While only ~2 nm (or 30%) Ag_2S

conversion on top and bottom facets is required. This difference is revealed only if during the design of the computational model we consider the two structural size parameters (*L* and *H*) separately, and consider it as an anisotropic change in the vertical *vs.* horizontal direction instead of an isotropic Ag_2S shell formation. The nature of this anisotropic behavior is due to differences in the sulfidation rate on different facets on the silver nanoprism.

Based on our computational analysis we hypothesize that a decrease in thickness of the Ag component (*i.e.,* replacing a few atomic layers of (111) on the top and bottom of the silver prism with Ag_2S layers) is the most likely explanation for the observed red-shifting of the nanoprisms during sulfidation.

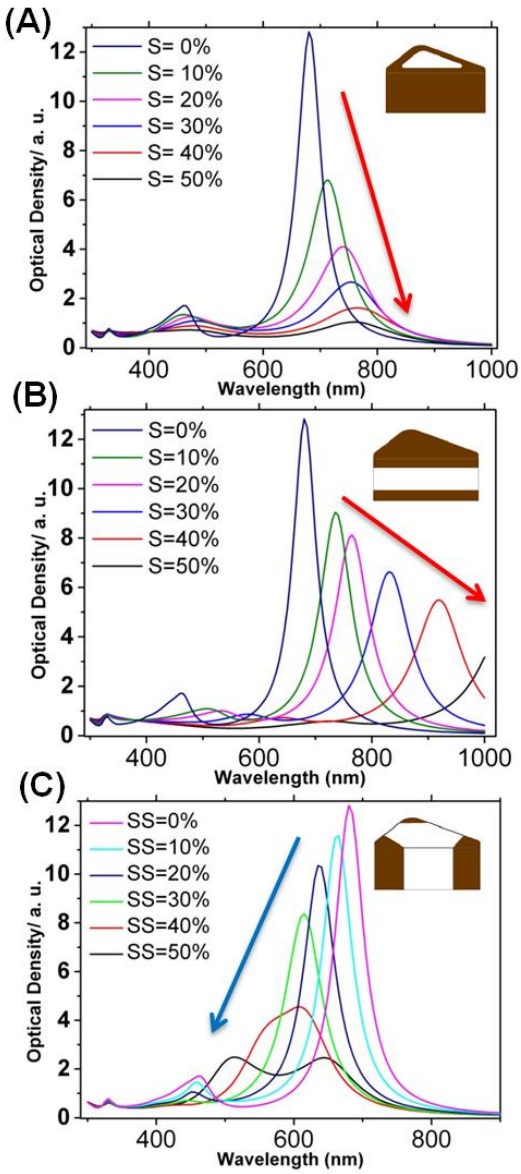

Figure 4. Calculated extinction spectra of a partially sulfidized Ag triangular prism on the edges, on the top and bottom facets and on the three tips. (A) Reduction in *L* generated by formation of triangular Ag_2S frame around the edges of silver component. (B) Reduction in *H* associated with formation of a Ag_2S-Ag-Ag_2S sandwich. (C) Increase in the *SS* value associated with conversion of tips to Ag_2S. Figure 4C is similar to Figure 2C and duplicated here only for better comparison purposes to panel A and B above. Relative values of Ag_2S conversion (*S* or *SS*) are given in the insets, considering a silver nanoprism with average edge length, height and tip curvature of 51, 7 and 6 nm, respectively, (collected from experimental data) with no Ag_2S at the tip of the nanoprism.

Experimental Characterization of the LSPR Red-Shift

To investigate our proposed pathway for the observed red-shifting as a consequence of high polysulfide concentration, we performed extensive TEM and XPS studies of the nanoprism structures. As the TEM measurements in Figure 5A-B indicate, the overall structure of each nanoprism is still crystalline after sulfidation, with the Ag_2S lattice structure at the tips of the nanoprism being clearly observable at higher magnification (Figure 5C). The fast Fourier transform (FFT) of the Ag_2S component is determined to be along the [4-11] zone axis of the Ag_2S crystal, but the (111) silver lattice was not recognizable in the HRTEM image even with different tilt angles. Interestingly, we found that the silver component of the Ag-Ag_2S nanoprism is not sensitive to high concentrations of H_2O_2 (37%), even though pure silver nanoprisms are etched rapidly under such conditions.[51] After introduction of 37% H_2O_2 to Ag-Ag_2S nanoprisms, many of the particles are completely intact and maintain their triangular morphology (Figure S3A-B), which is indirect evidence for the existence of a thin Ag_2S layer on (111) facets of the nanoprisms. In addition, there are tiny pieces of broken particles, which also indicates that the Ag_2S passivation layer is very thin and also contains imperfections; this is consistent with the known porosity of Ag_2S.[58]

In order to probe the reactivity of the (111) facets of the Ag nanoprism with S_x^{2-}, we synthesized edge-gold-coated silver nanoprisms (GSNP) according to the protocol introduced in earlier work.[59] These edge-gold-coated silver nanoprisms prevent diffusion of S_x^{2-} from tip and edge sites of the silver nanoprism. Surprisingly, we found that the sulfidation still occurs, but at a slightly lower rate as compared to bare Ag prisms. In GSNPs, since the gold nanoframe prevents the 69.9% expansion during transformation of Ag to Ag_2S, the final nanostructures are not

uniform and there are signs of collapse and cracking due to residual stress as depicted in Figures S3C-F.

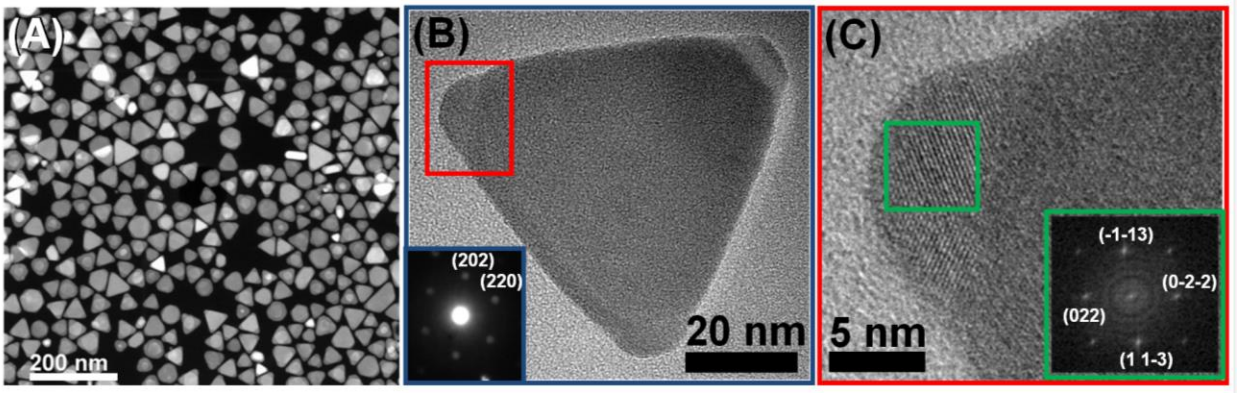

Figure 5. (A-B) Low magnification and single particle TEM image of a typical Ag-Ag_2S nanoprism (within high concentration Na_2S_x) at t = 1 min. Selected area diffraction pattern of the entire Ag-Ag_2S nanoprism shows a 6-fold hexagonal symmetry belonging to the silver component. (C) High resolution TEM image shows the Ag-Ag_2S nanoprism (taken from the red square box in panel B), which is along the [4-11] zone axis of Ag_2S and the [111] zone axis of the Ag component. Inset shows the FFT of the Ag_2S component.

The XPS etching experiment could not be performed on the samples prepared at low S_x^{2-} concentrations due to the small amount of sulfur in the particles. On the other hand, in the high concentration regime, since localized Ag_2S crystals are formed at the tips of the prisms, signals from the rest of the particles are not distinguishable and cannot confirm the existence of Ag_2S shell on the particles. Therefore, XPS etching analysis was carried out for particles made at intermediate polysulfide concentrations to probe the existence of the ultrathin Ag_2S layer as it was below the EDX detection limit.

When these triangular nanocrystals are sputtered with Ar^+ ions, the sulfur amount decreases after each etching step, thus confirming the core-isotropic shell morphology of the Ag-Ag_2S nanoprisms in the intermediate polysulfide concentration regime (Figures 6 and S4). This reinforces the notion of the existence of an ultrathin Ag_2S layer around a nanoprism. Based on experimental evidence and the simulations mentioned above, we conclude that the proper model for the Ag-Ag_2S hybrid system studied by Zeng *et al*.,[45] which is equal to the high polysulfide concentration case in our study, is a core (Ag) and anisotropic shell (Ag_2S) structure, in which the Ag_2S is thicker at the tips compared to the rest of the triangular facets.

Core-Anisotropic Shell Computational Model

Taking this new core-anisotropic shell model into account, new DDA simulations were performed with actual nanoprism dimensions to model the spectral evolution observed during the ensemble experiments. A uniform Ag_2S shell was assumed in the simulations, with an Ag_2S thickness that has been varied to optimize agreement with experiment since the exact thickness of the Ag_2S layer cannot be measured accurately in the experiment.

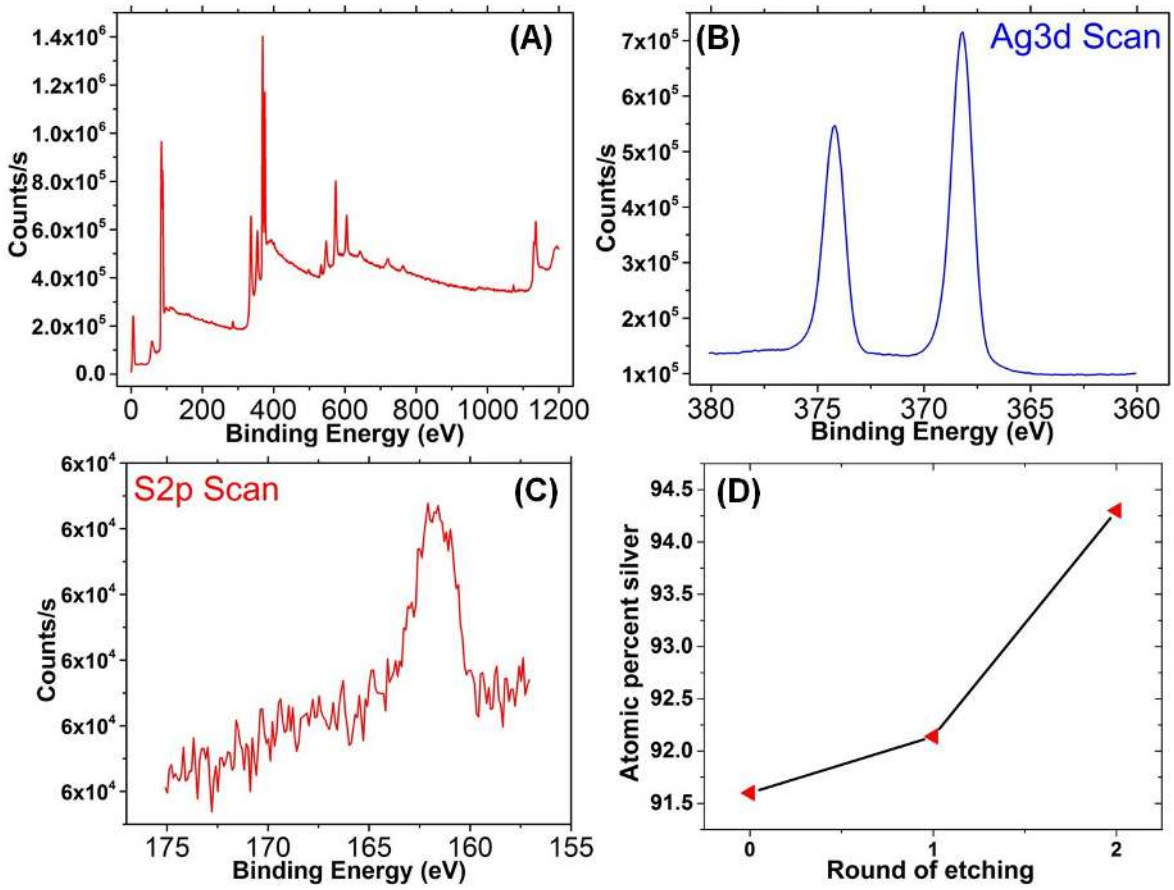

Figure 6. (A) X-ray photoelectron spectroscopy analysis of an Ag-Ag_2S nanoprism. Survey scan and high resolution scan related to (B) Ag3d and (C) S2p. (D) Plot of atomic percentage of Ag *versus* number of sputtering events shows an increase in the Ag concentration on the nanoprism surface with sequential Ar^+ sputtering. This data is consistent with the TEM observation in which the Ag_2S exists in the outermost layers of the Ag nanoprisms.

From Figure 2D it is clear that this model shows a red-shifting trend that closely matches the experimental results (Figure 2A), thereby corroborating our core-anisotropic shell model. The experimental SS values used in the DDA calculations (Figure 2D) show that the degree of tip conversion increases during the course of sulfidation. The same increasing trend of Ag_2S thickness on the (111) surface applies due to diffusion of extra sulfur ions in cracks between the Ag_2S on the (111) facets on top and bottom surfaces of the nanoprisms.

For sulfidation of the nanoprism in Figure 4C, we found that *SS* = 0, 18, 37 and 46%, fits the empirical data accurately. These SS values correspond to an Ag_2S shell thicknesses of 0, 0.6, 1.35 and 1.55 nm, which are approximately equivalent to 0, 3, 6 and 7 layers of reacted Ag atom layers on the (111) facets of the Ag nanoprism, respectively.

A phenomenon seen in both the experimental and calculated extinction spectra is the appearance of a new shoulder around 700 nm for *SS* = 46% (Figure- 2B,D, respectively). The theoretical calculation[60] indicates that this "shoulder" is actually a new SPR peak, which has been broadened due to interface damping (e.g., change in the dielectric function arising from surface scattering of free electrons near metal surface, an effect which has been considered in the current simulation). Our analysis suggests that this new LSPR peak, together with a peak around 850 nm, arises from plasmon hybridization induced by the dielectric substrate (Ag_2S corners), which is similar to the case of Ag nanocubes sitting on a glass substrate as studied by Schatz and Xia and co-workers,[61,62] and by Nordlander and co-workers.[63]

The calculated electric field distribution around the nanoprism is shown in Figure 7 for both the bare Ag nanoprism (*SS* = 0%, Figures 7A-F) and the Ag-Ag_2S hybrid structures with SS = 18% (Figure 7G-I). By examining the top-viewed near-field distribution of the pure Ag prism,

the in-plane dipole (Figures 7B-C) and quadrupole (Figure 7E-F) plasmonic mode can easily be identified.

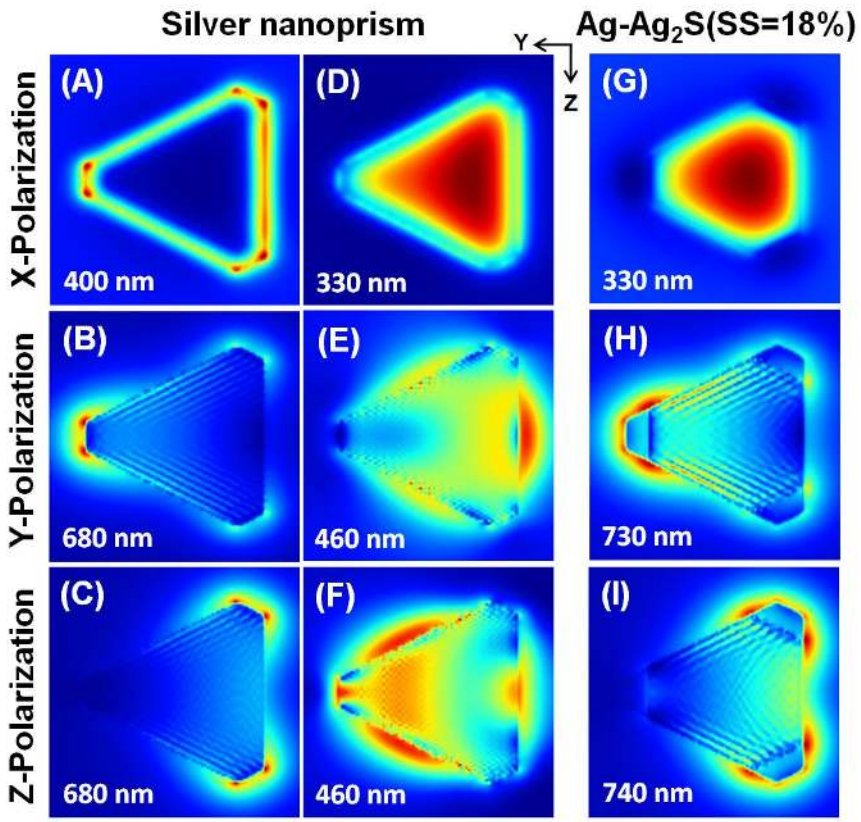

Figure 7. Near-field distribution calculated at different incident polarizations for (A-F) a pure silver nanoprism and (G-I) a Ag-Ag_2S hybrid nanoprism with *SS* = 18%. The near-field maps for the other SS values are reported in Figure S5-S9 in the Supporting Information.

One of the most promising applications of the current Ag-Ag_2S hybrid nanostructure is in plasmon-enhanced photocatalysis,[64-66] in which plasmon resonance excitation amplifies light absorption in the semiconductor region. As can be seen in Figure 7H-I, the in-plane dipole mode of the hexagonal silver core, which has the strongest extinction for the Ag-Ag_2S hybrid nanoprism, shows significant field enhancement in the Ag_2S tips. This suggests the possibility of efficient generation of electron-hole pairs in Ag_2S. One thing to note is that the "hot-spots" with the highest electric field intensity are located not only at the sharp tips of the on-resonance Ag hexagonal core, but also at the off-resonance Ag_2S corners. This indicates a strong electromagnetic interaction between these two adjacent components. Electric field distributions of the Ag-Ag_2S nanoprism at *SS* = 0, 18, 37 and 46% are animated using finite-difference time-domain (FDTD) as a function of wavelength in movies 1-4 in the Supporting Information.

By controlling the thickness of the nanoprisms and also adjusting the sulfidized section (*SS*), it is possible to not only fine-tune the interface size between the metal and semiconductor component, but also engineer both components' size and shape to reach maximum spectra overlap in this hybrid metal-semiconductor nanoprism. Near-field distributions calculated for other SS values are reported in Figure- S5-9.

Asymmetric Ag-Ag_2S Hybrid Nanoprisms

Silver nanoprisms have 3-fold rotational symmetry (C_3), but if one or two of the three tips is converted to a secondary phase (e.g., a semiconductor such as Ag_2S) the rotational symmetry is lowered to C_2. By applying this asymmetric design to Ag-Ag_2S hybrid structures, Ag-Ag_2S heterodimers can be created. This is achieved by using Na_2S instead of Na_2S_x in the synthesis.

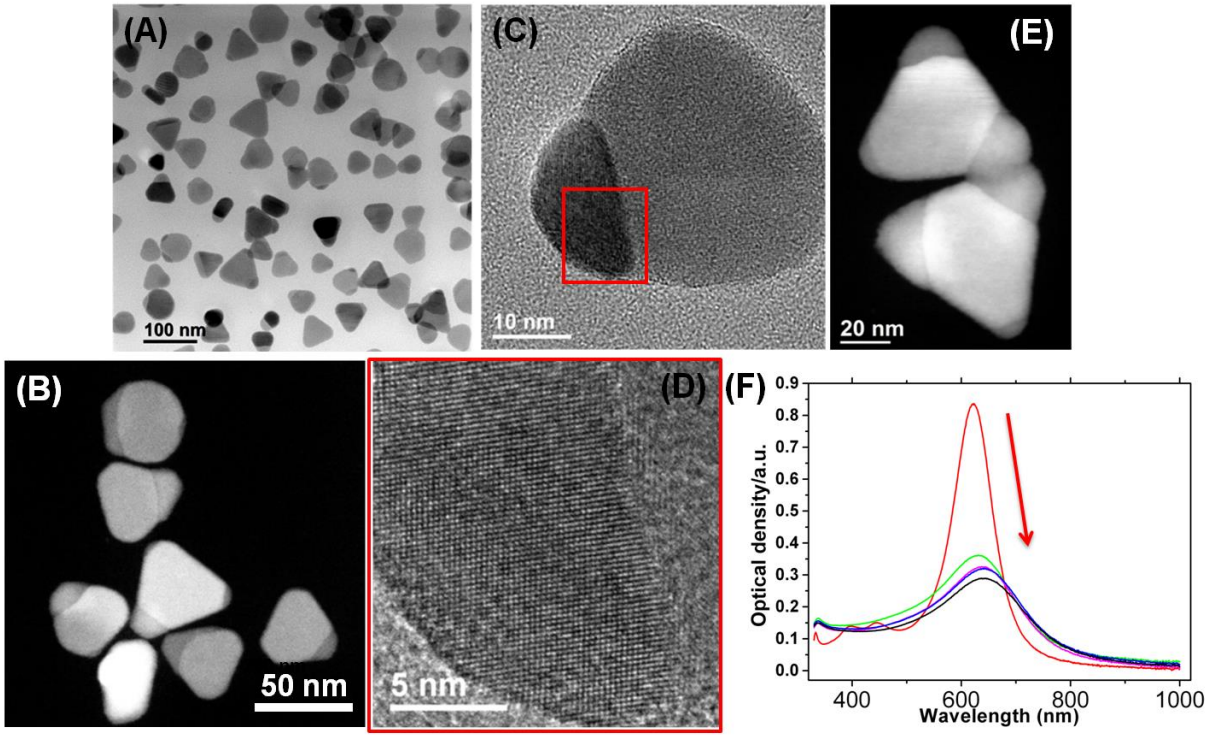

Figure 8. (A-D) TEM and STEM images of one-tip Ag-Ag_2S heterostructure obtained after the sulfidation reaction with Na_2S. (E) STEM images of two-tip Ag-Ag_2S heterostructures. There is a relatively small amount of Ag_2S on the third tip, which makes the sulfidation asymmetric. (F) UV-Vis spectra changes over the course of sulfidation of the ensemble Ag nanoprism by syringe pump infusion of 1 mM Na_2S at a rate of 5 mL/h.

One-tip and two-tip Ag-Ag_2S nanoprisms are depicted in Figure 8A-D and Figure 8E, respectively. As shown in Figure 8F the LSPR band of the Ag-Ag_2S nanoprisms red-shifts and the optical density decreases during the sulfidation process, similar to the symmetric conversion. However, the red-shift observed in one-tip and two-tip Ag-Ag_2S nanoprism conversion is smaller than what was observed in the symmetric case (Figure 2A). This asymmetric Ag_2S structure would likely alter the overall electronic structure, and thus, LSPR features of the Ag prisms, which may result in novel properties that symmetric prisms do not possess.[67]

Conclusion

We have elucidated the sulfidation process of Ag nanoprisms by combining experimental results, structural characterization and DDA calculations, leading to a new model that explains the LSPR evolution of the Ag-Ag_2S nanostructure during the reaction. This approach can serve as a model example to bridge two important families of inorganic nanostructures (*i.e.*, metals and semiconductors) to create new hybrid nanostructure with novel properties.

The progressive red- or blue-shifting of the dipole mode and the intensity evolution of the other plasmon modes are correlated with the structural changes during sulfidation, and the different behavior as a function of concentrations that can be inferred with the assistance of extensive DDA calculations (using dielectric functions for Ag and Ag_2S that are known from experiment, with no additional parameters needed). We also showed that, by using a Na_2S precursor, sulfidation can be controlled to make novel asymmetric Ag-Ag_2S nanoprisms. Given parallel reaction profiles, the results gained from our study can be extended to the preparation of other complex hybrid structures, including Ag-Ag_2Se and Au-Ag_2Te nanoprisms and other anisotropic metal-semiconductor nanostructures with rationally designed morphologies.

Materials and Methods

Preparation of Ag Nanoprism

The silver nanoprism preparation was carried out using a modified protocol based on previous reports[50,51,68,69] which is explained in the Supporting Information.

Preparation of edge gold-Coated Silver Nanoprisms (GSNPs)

The edge gold-coated silver nanoprisms (GSNPs) were synthesized by using our published protocol[51,59,70] with some modifications which is explained in details in the Supporting Information.

Sulfidation Reaction

The Na_2S_x solution was prepared by reacting aqueous Na_2S with sulfur powder according to a modified protocol reported by Jie *et al*.[45] In a typical process, 16 mg of sulfur powder was mixed and sonicated with 5.8 mL of 50 mM Na_2S aqueous solution for 60 min. The final concentration of sulfur should be around 135.4 mM in the final solution. This solution was heated in an oven held at 80 C for more than 12 h before use. In a typical process, 1-25 μL of the Na_2S_x solution was added to 5 mL of the aqueous suspension of silver nanoprisms under vigorous stirring at room temperature. The concentration of silver nanoprism is estimated to be ~180 μM. The reaction was quenched at a specific time point by centrifugation of the solution at 14,000 rpm for 3 min following by re-dispersing in Nanopure water.

X-Ray Photoelectron Spectroscopy (XPS) Analysis

XPS was conducted with a Thermo Scientific ESCA Lab 250Xi XPS with a monochromatic KR Al X-ray line using an aluminum anode (1486.6 eV) at 225 W. The probe size was 500 μm in diameter, nominally elliptical in cross-section. A charge neutralization flood gun (Ar^+ ions) was used to compensate for local electrostatic fields on the Ag-Ag_2S nanodisc

particles with homogenous Ag_2S shell. Samples for XPS are prepared by drop-casting solutions of Ag nanoprisms on a PEI functionalized SiO_2 substrate to force them to lay down on the substrate and avoid agglomeration upon drying. A dwell time of 100 ms and 5 scans of C, 10 scans of Ag and S are used in our study.

Discrete Dipole Approximation (DDA) Simulations

We employ DDSCAT,[71] an open-source code based on the Discrete Dipole Approximation (DDA).[72-75] The Gutkowicz-Krusin and Draine lattice dispersion relation (GKD-LDR)[76] was adopted to relate the macroscopic dielectric function of the bulk material to the microscopic polarizability of the dipoles. The optical constants for Ag are from a compilation by Lynch and Hunter,[77] and that for Ag_2S is from Bennett and co-workers.[78] Ag_2S in the lattice work was studied using silver tarnish, and it was found that although Ag_2S is transparent at wavelengths longer than 1.4 μm, in the visible it a somewhat lossy semiconductor, with $n + ik \approx 3.1 + 0.8i$ near 500 nm.

The interband transition of Ag_2S is not ignored in this study. As described above, empirical optical constants from previous experiments were adopted in our theoretical simulation, which capture the interband transition effect of Ag_2S to the extinction spectrum. The Ag_2S's absorption is located in the visible range, consistent with what is shown in the literature. However, in this experiment, Ag_2S acts mostly as an optical-inactive high-refractive-index medium and its contribution to the extinction spectrum is almost negligible, due to much stronger interaction between the metallic (Ag) component and the electromagnetic field.

The surface scattering effect was included by adjusting the Drude damping term Υ following the "1/*R*" law, where *R* is the effective mean free path of electron.[79] Various models for the calculation of *R* have been proposed;[80,81] but this work follows the method adopted in an

earlier paper[57] by this group where the prism thickness is excluded from the evaluation as surface scattering was found to be coherent for the flat surfaces of the prisms. A water environment was assumed, with a refractive index of 1.33. The calculated extinction spectra were averaged over the three principal polarization directions before being compared with experimental UV-Vis spectra. The near-field of the triangular prism was calculated using a method proposed by Flatau and Draine.[75]

The structural parameters used in nanoprism modeling were derived from TEM measurements. The prism thickness H was taken to be 7 nm. The triangular face has an average side length L = 51 nm, and the three corners were observed to be rounded off with a radius R = 6 nm. In the DDA calculations, the nanoprism was represented by a cubic array of point dipoles with inter-dipole spacing of 0.4 nm. Convergence tests showed that this value can guarantee a reasonable balance between numerical accuracy and computational cost.

The coordinate system describing the polarization of the incident electric field is defined such that each coordinate axis is along one principle axis of the prism, e.g., the x-axis is along the threefold symmetry axis of prism, the y-axis along one bisector of the triangular face.

Supporting Information. DDA simulation results and spectroscopic data for a wider range of particles and additional electron microscopy images. This material is available free of charge *via* the Internet at http://pubs.acs.org

AUTHOR INFORMATION

Corresponding Author

*chadnano@northwestern.edu, *g-schatz@northwestern.edu

Author Contributions

The manuscript was written through contributions of all authors. All authors have given approval to the final version of the manuscript. ¶These authors contributed equally.

ACKNOWLEDGMENT

C.A.M, M.M.S and G.C.S gratefully acknowledge financial support by the following awards: AFOSR award FA9550-12-1-0280, and NSF's MRSEC program (DMR-1121262) at the Materials Research Center of Northwestern University. M.M.S also acknowledges the SINGA fellowship by Singapore Agency for Science, Technology and Research (A*STAR) and Nanyang Technological University Postdoctoral Fellowship supported by Institute of Nano-System Interface Science &Technology (INSIST). N.Z and N.L acknowledge DOE- BES grant: DOE DE-FG02-10ER16153. Y.Z and Z.C. were supported by the National Natural Science Foundation of China (21503001, 61475001). Computing resources were provided by the Quest high performance computing facility at Northwestern University. This work made use of the EPIC facility (NUANCE Center-Northwestern University), which has received support from the MRSEC program (NSF DMR-1121262) at the Materials Research Center; the International Institute for Nanotechnology (IIN); and the State of Illinois, through the IIN.

References

1. Yang, J.; Sargent, E.; Kelley, S.; Ying, J. Y., A General Phase-Transfer Protocol for Metal Ions and Its Application in Nanocrystal Synthesis. *Nat. Mater.* **2009**, 8, 683-689.

2. Pang, M.; Hu, J.; Zeng, H. C., Synthesis, Morphological Control, and Antibacterial Properties of Hollow/Solid Ag_2S/Ag Heterodimers. *J. Am. Chem. Soc.* **2010**, 132, 10771-10785.

3. Liu, B.; Ma, Z., Synthesis of Ag_2S–Ag Nanoprisms and Their Use as DNA Hybridization Probes. *Small* **2011**, 7, 1587-1592.

4. Kryukov, A. I.; Stroyuk, A. L.; Zin'chuk, N. N.; Korzhak, A. V.; Kuchmii, S. Y., Optical and Catalytic Properties of Ag_2S Nanoparticles. *J. Mol. Catal. A: Chem.* **2004**, 221, 209-221.

5. Motte, L.; Urban, J., Silver Clusters on Silver Sulfide Nanocrystals: Synthesis and Behavior after Electron Beam Irradiation. *J. Phys. Chem. B* **2005**, 109, 21499-21501.

6. Terabe, K.; Nakayama, T.; Hasegawa, T.; Aono, M., Formation and Disappearance of a Nanoscale Silver Cluster Realized by Solid Electrochemical Reaction. *J. Appl. Phys.* **2002**, 91, 10110-10114.

7. Mokari, T.; Rothenberg, E.; Popov, I.; Costi, R.; Banin, U., Selective Growth of Metal Tips onto Semiconductor Quantum Rods and Tetrapods. *Science* **2004**, 304, 1787-1790.

8. Shaviv, E.; Banin, U., Synergistic Effects on Second Harmonic Generation of Hybrid CdSe−Au Nanoparticles. *ACS Nano* **2010**, 4, 1529-1538.

9. Lee, J.-S.; Shevchenko, E. V.; Talapin, D. V., Au−PbS Core−Shell Nanocrystals: Plasmonic Absorption Enhancement and Electrical Doping *via* Intra-particle Charge Transfer. *J. Am. Chem. Soc.* **2008**, 130, 9673-9675.

10. Lee, J.; Hernandez, P.; Lee, J.; Govorov, A. O.; Kotov, N. A., Exciton–Plasmon Interactions in Molecular Spring Assemblies of Nanowires and Wavelength-Based Protein Detection. *Nat. Mater.* **2007**, 6, 291 - 295.

11. Zhang, J.; Yun Tang; Lee, K.; Ouyang, M., Tailoring Light–Matter–Spin Interactions in Colloidal Hetero-Nanostructures. *Nature* **2010**, 466, 91-95.

12. Khon, E.; Mereshchenko, A.; Tarnovsky, A. N.; Acharya, K.; Klinkova, A.; Hewa-Kasakarage, N. N.; Nemitz, I.; Zamkov, M., Suppression of the Plasmon Resonance in Au/CdS Colloidal Nanocomposites. *Nano Lett.* **2011**, 11, 1792-1799.

13. Wang, D.; Li, Y., One-Pot Protocol for Au-Based Hybrid Magnetic Nanostructures *via* a Noble-Metal-Induced Reduction Process. *J. Am. Chem. Soc.* **2010**, 132, 6280-6281.

14. Choi, S.-H.; Kim, E.-G.; Hyeon, T., One-Pot Synthesis of Copper−Indium Sulfide Nanocrystal Heterostructures with Acorn, Bottle, and Larva Shapes. *J. Am. Chem. Soc.* **2006**, 128, 2520-2521.

15. Mokari, T.; Sztrum, C. G.; Salant, A.; Rabani, E.; Banin, U., Formation of Asymmetric One-sided Metal-Tipped Semiconductor Nanocrystal Dots and Rods. *Nat. Mater.* **2005**, 4, 855-863.

16. Jin, Y.; Gao, X., Plasmonic Fluorescent Quantum Dots. *Nat. Nanotechnol.* **2009**, 4, 571-576.

17. Alivisatos, A. P., Perspectives on the Physical Chemistry of Semiconductor Nanocrystals. *J. Phys. Chem.* **1996**, 100, 13226-13239.

18. Eustis, S.; El-Sayed, M. A., Why Gold Nanoparticles Are More Precious than Pretty Gold: Noble Metal Surface Plasmon Resonance and Its Enhancement of the Radiative and

Nonradiative Properties of Nanocrystals of Different Shapes. *Chem. Soc. Rev.* **2006**, 35, 209-217.

19. Sheldon, M. T.; Trudeau, P.-E.; Mokari, T.; Wang, L.-W.; Alivisatos, A. P., Enhanced Semiconductor Nanocrystal Conductance *via* Solution Grown Contacts. *Nano Lett.* **2009**, 9, 3676-3682.

20. Kamat, P. V., Quantum Dot Solar Cells. Semiconductor Nanocrystals as Light Harvesters. *J. Phys. Chem. C* **2008**, 112, 18737-18753.

21. Shemesh, Y.; Macdonald, J. E.; Menagen, G.; Banin, U., Synthesis and Photocatalytic Properties of a Family of CdS-PdX Hybrid Nanoparticles. *Angew. Chem. Int. Ed.* **2011**, 50, 1185-1189.

22. Zhao, N.; Vickery, J.; Guerin, G.; Park, J. I.; Winnik, M. A.; Kumacheva, E., Self-Assembly of Single-Tip Metal–Semiconductor Nanorods in Selective Solvents. *Angew. Chem. Int. Ed.* **2011**, 50, 4606-4610.

23. Pacholski, C.; Kornowski, A.; Weller, H., Site-Specific Photodeposition of Silver on ZnO Nanorods. *Angew. Chem. Int. Ed.* **2004**, 43, 4774-4777.

24. Dukovic, G.; Merkle, M. G.; Nelson, J. H.; Hughes, S. M.; Alivisatos, A. P., Photodeposition of Pt on Colloidal CdS and CdSe/CdS Semiconductor Nanostructures. *Adv. Mater.* **2008**, 20, 4306-4311.

25. Habas, S. E.; Yang, P.; Mokari, T., Selective Growth of Metal and Binary Metal Tips on CdS Nanorods. *J. Am. Chem. Soc.* **2008**, 130, 3294-3295.

26. Yang, J.; Ying, J. Y., Nanocomposites of Ag_2S and Noble Metals. *Angew. Chem. Int. Ed.* **2011**, 50, 4637-4643.

27. Jing, H.; Large, N.; Zhang, Q.; Wang, H., Epitaxial Growth of Cu_2O on Ag Allows for Fine Control Over Particle Geometries and Optical Properties of Ag–Cu_2O Core–Shell Nanoparticles. *J. Phys. Chem. C* **2014**, 118, 19948-19963.

28. Liu, M.; Guyot-Sionnest, P., Preparation and Optical Properties of Silver Chalcogenide Coated Gold Nanorods. *J. Mater. Chem.* **2006**, 16, 3942-3945.

29. Som, A.; Samal, A. K.; Udayabhaskararao, T.; Bootharaju, M. S.; Pradeep, T., Manifestation of the Difference in Reactivity of Silver Clusters in Contrast to Its Ions and Nanoparticles: The Growth of Metal Tipped Te Nanowires. *Chem. Mat.* **2014**, 26, 3049-3056.

30. Lim, W. P.; Zhang, Z.; Low, H. Y.; Chin, W. S., Preparation of Ag_2S Nanocrystals of Predictable Shape and Size. *Angew. Chem. Int. Ed.* **2004**, 43, 5685-5689.

31. Ivanov-Shitz, A. K., Computer Simulation of Superionic Conductors: II. Cationic Conductors. Review. *Crystallogr. Rep.* **2007**, 52, 302-315.

32. Lei, Y.; Jia, H.; He, W.; Zhang, Y.; Mi, L.; Hou, H.; Zhu, G.; Zheng, Z., Hybrid Solar Cells with Outstanding Short-Circuit Currents Based on a Room Temperature Soft-Chemical Strategy: The Case of P3HT:Ag_2S. *J. Am. Chem. Soc.* **2012**, 134, 17392-17395.

33. Chang, S.; Li, Q.; Xiao, X.; Wong, K. Y.; Chen, T., Enhancement of Low Energy Sunlight Harvesting in Dye-Sensitized Solar Cells Using Plasmonic Gold Nanorods. *Energy Environ. Sci.* **2012**, 5, 9444-9448.

34. Yang, W.; Zhang, L.; Hu, Y.; Zhong, Y.; Wu, H. B.; Lou, X. W., Microwave-Assisted Synthesis of Porous Ag_2S–Ag Hybrid Nanotubes with High Visible-Light Photocatalytic Activity. *Angew. Chem. Int. Ed.* **2012**, 51, 11501-11504.

35. Meng, Z.-D.; Ghosh, T.; Zhu, L.; Choi, J.-G.; Park, C.-Y.; Oh, W.-C., Synthesis of Fullerene Modified with Ag_2S with High Photocatalytic Activity under Visible Light. *J. Mater. Chem.* **2012**, 22, 16127-16135.

36. Nagasuna, K.; Akita, T.; Fujishima, M.; Tada, H., Photodeposition of Ag_2S Quantum Dots and Application to Photoelectrochemical Cells for Hydrogen Production under Simulated Sunlight. *Langmuir* **2011**, 27, 7294-7300.

37. Hodes, G.; Manssen, J.; Cahen, D., Photoelectrochemical Energy Conversion and Storage Using Polycrystalline Chalcogenide Electrodes. *Nature* **1976**, 261, 403-404.

38. Wang, R. Y.; Tangirala, R.; Raoux, S.; Jordan-Sweet, J. L.; Milliron, D. J., Ionic and Electronic Transport in Ag_2S Nanocrystal–GeS_2 Matrix Composites with Size-Controlled Ag_2S Nanocrystals. *Adv. Mater.* **2012**, 24, 99-103.

39. Liang, C.; Terabe, K.; Hasegawa, T.; Negishi, R.; Tamura, T.; Aono, M., Ionic–Electronic Conductor Nanostructures: Template-Confined Growth and Nonlinear Electrical Transport. *Small* **2005**, 1, 971-975.

40. Xu, Z.; Bando, Y.; Wang, W.; Bai, X.; Golberg, D., Real-Time *In Situ* HRTEM-Resolved Resistance Switching of Ag_2S Nanoscale Ionic Conductor. *ACS Nano* **2010**, 4, 2515-2522.

41. Hong, G.; Robinson, J. T.; Zhang, Y.; Diao, S.; Antaris, A. L.; Wang, Q.; Dai, H., In Vivo Fluorescence Imaging with Ag_2S Quantum Dots in the Second Near-Infrared Region. *Angew. Chem. Int. Ed.* **2012**, 51, 9818-9821.

42. Zhang, Y.; Hong, G.; Zhang, Y.; Chen, G.; Li, F.; Dai, H.; Wang, Q., Ag_2S Quantum Dot: A Bright and Biocompatible Fluorescent Nanoprobe in the Second Near-Infrared Window. *ACS Nano* **2012**, 6, 3695-3702.

43. Du, Y.; Xu, B.; Fu, T.; Cai, M.; Li, F.; Zhang, Y.; Wang, Q., Near-Infrared Photoluminescent Ag_2S Quantum Dots from a Single Source Precursor. *J. Am. Chem. Soc.* **2010**, 132, 1470-1471.

44. Fang, C.; Lee, Y. H.; Shao, L.; Jiang, R.; Wang, J.; Xu, Q.-H., Correlating the Plasmonic and Structural Evolutions during the Sulfidation of Silver Nanocubes. *ACS Nano* **2013**, 7, 9354-9365.

45. Zeng, J.; Tao, J.; Su, D.; Zhu, Y.; Qin, D.; Xia, Y., Selective Sulfuration at the Corner Sites of a Silver Nanocrystal and Its Use in Stabilization of the Shape. *Nano Lett.* **2011**, 3010-3015.

46. Jin, R.; Cao, Y.; Mirkin, C. A.; Kelly, K.; Schatz, G. C.; Zheng, J., Photoinduced Conversion of Silver Nanospheres to Nanoprisms. *Science* **2001**, 294, 1901-1903.

47. Kelly, K. L.; Coronado, E.; Zhao, L. L.; Schatz, G. C., The Optical Properties of Metal Nanoparticles: The Influence of Size, Shape, and Dielectric Environment. *J. Phys. Chem. B* **2003**, 107, 668-677.

48. Xue, C.; Metraux, G. S.; Millstone, J. E.; Mirkin, C. A., Mechanistic Study of Photomediated Triangular Silver Nanoprism Growth. *J. Am. Chem. Soc.* **2008**, 130, 8337-8344.

49. Jin, R. C.; Cao, Y. C.; Hao, E. C.; Metraux, G. S.; Schatz, G. C.; Mirkin, C. A., Controlling Anisotropic Nanoparticle Growth through Plasmon Excitation. *Nature* **2003**, 425, 487-490.

50. Shahjamali, M. M.; Bosman, M.; Cao, S.; Huang, X.; Saadat, S.; Martinsson, E.; Aili, D.; Tay, Y. Y.; Liedberg, B.; Loo, S. C. J.; Zhang, H.; Boey, F.; Xue, C., Gold Coating of Silver Nanoprisms. *Adv. Funct. Mater.* **2012**, 22, 849-854.

51. Shahjamali, M. M.; Bosman, M.; Cao, S.; Huang, X.; Cao, X.; Zhang, H.; Pramana, S. S.; Xue, C., Surfactant-Free Sub-2 nm Ultrathin Triangular Gold Nanoframes. *Small* **2013**, 9, 2880-2886.

52. Buschmann, V.; Van Tendeloo, G.; Monnoyer, P.; Nagy, J. B., Structural Characterization of Colloidal Ag_2Se Nanocrystals. *Langmuir* **1998**, 14, 1528-1531.

53. Hao, E.; Schatz, G. C.; Hupp, J. T., Synthesis and Optical Properties of Anisotropic Metal Nanoparticles. *J. Fluoresc.* **2004**, 14, 331-341.

54. Shuford, K. L.; Ratner, M. A.; Schatz, G. C., Multipolar Excitation in Triangular Nanoprisms. *J. Chem. Phys.* **2005**, 123, 114713.

55. Sherry, L. J.; Jin, R.; Mirkin, C. A.; Schatz, G. C.; Van Duyne, R. P., Localized Surface Plasmon Resonance Spectroscopy of Single Silver Triangular Nanoprisms. *Nano Lett.* **2006**, 6, 2060-2065.

56. Boneberg, J.; König-Birk, J.; Münzer, H.-J.; Leiderer, P.; Shuford, K. L.; Schatz, G. C., Optical Near-Fields of Triangular Nanostructures. *Appl. Phys. A* **2007**, 89, 299-303.

57. Blaber, M. G.; Henry, A.-I.; Bingham, J. M.; Schatz, G. C.; Van Duyne, R. P., LSPR Imaging of Silver Triangular Nanoprisms: Correlating Scattering with Structure Using Electrodynamics for Plasmon Lifetime Analysis. *J. Phys. Chem. C* **2011**, 116, 393-403.

58. Wang, D.; Xie, T.; Peng, Q.; Li, Y., Ag, Ag_2S, and Ag_2Se Nanocrystals: Synthesis, Assembly, and Construction of Mesoporous Structures. *J. Am. Chem. Soc.* **2008**, 130, 4016-4022.

59. Shahjamali, M. M.; Salvador, M.; Bosman, M.; Ginger, D. S.; Xue, C., Edge-Gold-Coated Silver Nanoprisms: Enhanced Stability and Applications in Organic Photovoltaics and Chemical Sensing. *J. Phys. Chem. C* **2014**, 118, 12459-12468.

60. Zhou, Y.; Schatz, G. C., Dielectric-Substrate-Induced Hybridization of Localized Surface Plasmon Mode in Ag/Ag_2S Hybrid Nanoprism. Unpublished work, 2016.

61. Sherry, L. J.; Chang, S.-H.; Schatz, G. C.; Van Duyne, R. P.; Wiley, B. J.; Xia, Y., Localized Surface Plasmon Resonance Spectroscopy of Single Silver Nanocubes. *Nano Lett.* **2005**, 5, 2034-2038.

62. McMahon, J. M.; Wang, Y.; Sherry, L. J.; Van Duyne, R. P.; Marks, L. D.; Gray, S. K.; Schatz, G. C., Correlating the Structure, Optical Spectra, and Electrodynamics of Single Silver Nanocubes. *J. Phys. Chem. C* **2009**, 113, 2731-2735.

63. Zhang, S.; Bao, K.; Halas, N. J.; Xu, H.; Nordlander, P., Substrate-Induced Fano Resonances of a Plasmonic Nanocube: A Route to Increased-Sensitivity Localized Surface Plasmon Resonance Sensors Revealed. *Nano Lett.* **2011**, 11, 1657-1663.

64. Hou, W.; Cronin, S. B., A Review of Surface Plasmon Resonance-Enhanced Photocatalysis. *Adv. Funct. Mater.* **2013**, 23, 1612-1619.

65. Zhang, X.; Chen, Y. L.; Liu, R.-S.; Tsai, D. P., Plasmonic Photocatalysis. *Rep. Prog. Phys.* **2013**, 76, 046401.

66. Warren, S. C.; Thimsen, E., Plasmonic Solar Water Splitting. *Energy Environ. Sci.* **2012**, 5, 5133-5146.

67. Liang, S.; Liu, X.-L.; Yang, Y.-Z.; Wang, Y.-L.; Wang, J.-H.; Yang, Z.-J.; Wang, L.-B.; Jia, S.-F.; Yu, X.-F.; Zhou, L.; Wang, J.-B.; Zeng, J.; Wang, Q.-Q.; Zhang, Z., Symmetric and Asymmetric Au–AgCdSe Hybrid Nanorods. *Nano Lett.* **2012**, 12, 5281-5286.

68. Martinsson, E.; Otte, M. A.; Shahjamali, M. M.; Sepulveda, B.; Aili, D., Substrate Effect on the Refractive Index Sensitivity of Silver Nanoparticles. *J. Phys. Chem. C* **2014**, 118, 24680-24687.

69. Shahjamali, M. M.; Lim Ming, P.; Kathawala, M. H.; Pratheepan, S.; Saini, N. B.; Mansor, M. B.; Can, X. *Triangular Core-Shell Structure Ag@AgAu*, Photonics Global Conference (PGC), 2010, 14-16 Dec. 2010; 2010; pp 1-3.

70. Shahjamali, M. M.; Martinsson, E.; Marcello, W.; Yin, L.; Liedberg, B.; Boey, F.; Xue, C. *Edge Gold-Coated Silver Nanoprism [Ag@(Au Nanoframe)] for H_20_2 Detection*, Proc. SPIE 8351, Third Asia Pacific Optical Sensors Conference, 2012; pp 83511S-83511S-5.

71. Draine, B. T.; Flatau, P. J., User Guide for the Discrete Dipole Approximation Code DDSCAT 7.3. 2013, arXiv:1305.6497. arXiv.org e-Print archive. http:// arXiv:1305.6497v1 (accessed Mar 23, 2016).

72. Draine, B. T.; Goodman, J., Beyond Clausius-Mossotti: Wave Propagation on a Polarizable Point Lattice and the Discrete Dipole Approximation. *Astrophys. J.* **1993**, 405, 685-697.

73. Draine, B. T.; Flatau, P. J., Discrete-Dipole Approximation For Scattering Calculations. *J. Opt. Soc. Am. A* **1994**, 11, 1491-1499.

74. Yurkin, M. A.; Hoekstra, A. G., The Discrete Dipole Approximation: An Overview and Recent Developments. *J. Quant. Spectrosc. Radiat. Transfer* **2007**, 106, 558-589.

75. Flatau, P. J.; Draine, B. T., Fast Near Field Calculations in the Discrete Dipole Approximation for Regular Rectilinear Grids. *Opt. Express* **2012**, 20, 1247-1252.

76. Gutkowicz-Krusin, D.; Draine, B. T., Propagation of Electromagnetic Waves on a Rectangular Lattice of Polarizable Points. 2004, arXiv:astro-ph/0403082. arXiv.org e-Print archive. http://arxiv.org/abs/astro-ph/0403082v1 (accessed Mar 23, 2016).

77. Lynch, D. W.; Hunter, W. R., Comments on the Optical Constants of Metals and an Introduction to the Data for Several Metals. In *Handbook of Optical Constants of Solids*, Palik, E. D., Ed. Academic Press: New York, 1985; Vol. 1.

78. Bennett, J. M.; Stanford, J.; Ashley, E., Optical Constants of Silver Sulfide Tarnish Films. *J. Opt. Soc. Am.* **1970**, 60, 224-231.

79. Kreibig, U.; Vollmer, M., *Optical Properties of Metal Clusters*. Springer-Verlag: Berlin Heidelberg, Germany, 1995.

80. Coronado, E. A.; Schatz, G. C., Surface Plasmon Broadening for Arbitrary Shape Nanoparticles: A Geometrical Probability Approach. *J. Chem. Phys.* **2003**, 119, 3926-3934.

81. Moroz, A., Electron Mean Free Path in a Spherical Shell Geometry. *J. Phys. Chem. C* **2008**, 112, 10641-10652.

Table of contents graphic

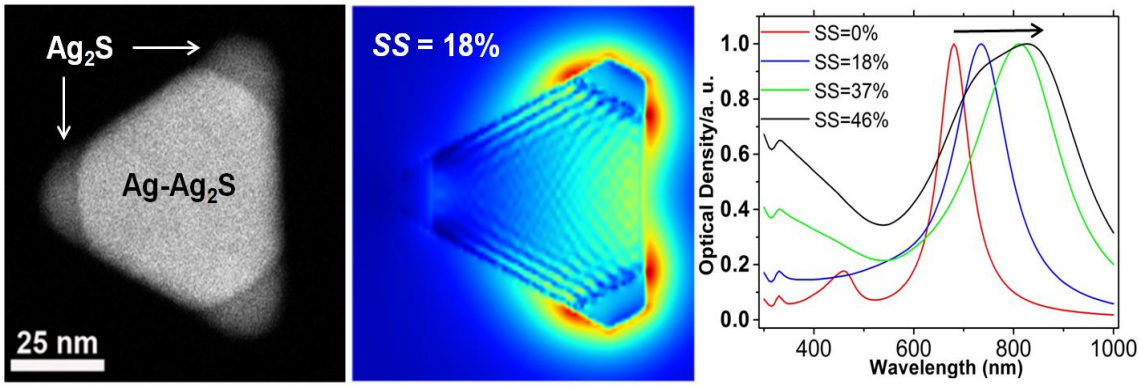

Evolution of the structure and extinction spectra of Ag nanoprisms during the sulfidation process is investigated theoretically and experimentally. Surprisingly, it was found that Ag_2S can form both on the tips and on the triangular (111) surfaces of the prisms, leading to a core-anisotropic shell Ag-A_2S nanoprism structure in which the plasmon can blue- or red-shift. Interestingly, the "hot-spots" with highest electric field intensity are located not only at the tips of the on-resonance Ag hexagonal core but also at the off-resonance Ag_2S tips, indicating strong electromagnetic interaction between the Ag and Ag_2S components.